Missouri University of Science and Technology
Scholars' Mine

Mechanical and Aerospace Engineering Faculty Research & Creative Works

Mechanical and Aerospace Engineering

01 Jan 1975

Thermal Stresses In A Sphere Due To Local Heating Followed By Complete Cooling

T. S. Chen
Missouri University of Science and Technology, tschen@mst.edu

K. Thirumalai

J. B. Cheung

Follow this and additional works at: https://scholarsmine.mst.edu/mec_aereng_facwork

 Part of the Aerospace Engineering Commons, and the Mechanical Engineering Commons

Recommended Citation

T. S. Chen et al., "Thermal Stresses In A Sphere Due To Local Heating Followed By Complete Cooling," *Journal of Heat Transfer*, vol. 97, no. 1, pp. 145 - 148, American Society of Mechanical Engineers, Jan 1975.
The definitive version is available at https://doi.org/10.1115/1.3450269

This Article - Journal is brought to you for free and open access by Scholars' Mine. It has been accepted for inclusion in Mechanical and Aerospace Engineering Faculty Research & Creative Works by an authorized administrator of Scholars' Mine. This work is protected by U. S. Copyright Law. Unauthorized use including reproduction for redistribution requires the permission of the copyright holder. For more information, please contact scholarsmine@mst.edu.

Check for updates

Table 1

Test description flux shape—spacer grid type	CHF scaling constant K
$u \sin u$—simple support grid	1.52
$u \sin u$—mixing grid A	1.52
$\cos u$—mixing grid B	1.66

K were found to be independent of pressure. The calculated values of the CHF scaling constant are presented in Table 1.

The measured CHF in water was then compared with the predicted CHF based on the values of c_1 from R-11 and the scaling constant from Table 1. These comparisons are presented in Figs. 1 and 2.

Discussion

Since K (Table 1) was not a unique constant—1.52 for the u sine u test section and 1.66 for the cos u test section—it is recognized that we still do not have a generalized model for different axial flux shapes in the subcooled boiling regime. While we still need both water and refrigerant data, there are a number of reasons why refrigerant tests are valuable. First, in some instances due to power limitations, only low inlet subcooling CHF data can be taken. In this case, the refrigerant data is used to predict CHF with highly subcooled inlet conditions. Second, refrigerant tests are considerably cheaper due to power savings and reduced test section maintenance costs.

The refrigerant tests can also be used to predict changes in CHF as a result of changes in grids. For example, referring to Fig. 1, refrigerant tests scaled the water results using the same scaling constant *(K)* for simple support grids and mixing grids. This indicates that changing grid types has the same effect in Freon as in water and that a designer may be able to optimize the rod bundle thermal hydraulics with refrigerant tests and then verify the end result with water.

References

1 Coeffield, R. D., Jr., Rohrer, W. M., Jr., and Tong, L. S., "A Subcooled DNB Investigation of Freon-113 and Its Similarity to Subcooled Water DNB Data," Nuclear Engineering and Design, May 19, 1969, pp. C-1–C-11.

2 Motley, F. E., Cadek, F. F., Cermak, J. O., Tong, L. S., Gouse, S. W., Paul, F., and Purcupile, J. C., "CHF Data From Freon-11 Flow for Scaling CHF in Water," International Symposium on Two-Phase Systems, Haifa, Israel, 1971.

3 Stevens, G. F., and Kirby, G. J., "A Quantitative Comparison Between Burnout Data for Water at 1000 psia and Freon-12 at 155 psia. Uniformly Heated Round Tubes, Vertical Upflow," AEEW-R327, 1964.

4 Levy, S., "Forced Convection Subcooled Boiling—Prediction of Vapor Volumetric Fraction," *International Journal of Heat and Mass Transfer*, Vol. 10, Pergamon Press, Great Britain, 1967, pp 951–965.

5 Rosal, E. R., Cermak, J. O., Tong, L. S., Casterline, J. E., and Matzner, B., "Rod Bundle Axial Non-Uniform Heat Flux DNB Tests and Data (under preparation)."

6 Purcupile, J. C., and Gouse, S. W., Jr., "Reynolds Flux Model of Critical Heat Flux in Subcooled Forced Convection Boiling," ASME Paper No. 72-HT-4.

7 Purcupile, J. C., Tong, L. S. and Gouse, S. W., Jr., "Refrigerant—Water Scaling of Critical Heat Flux in Round Tubes—Subcooled Forced Convection Boiling," JOURNAL OF HEAT TRANSFER, TRANS. ASME, Series C, Vol. 55, May 1973.

8 Rowe, D. S., "Cobra III: A Digital Computer Program for Steady State and Transient Thermal-Hydraulic Analysis of Rod Bundle Nuclear Fuel Elements," BNWL-B-82.

9 Armand, A. A., "The Resistance During the Movement of a Two-Phase System in Horizontal Pipes," AERE Trans 828 Izvestiya Vsesojuznogo Teplolekhechaskogo Instituta 1946.

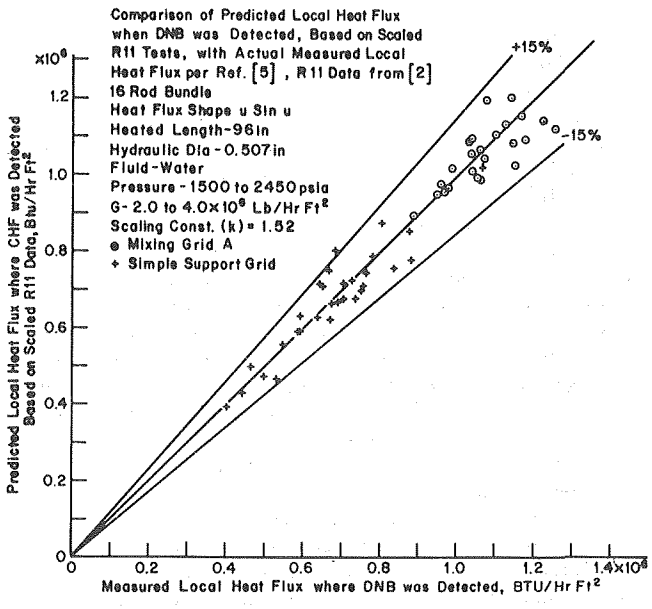

Fig. 1

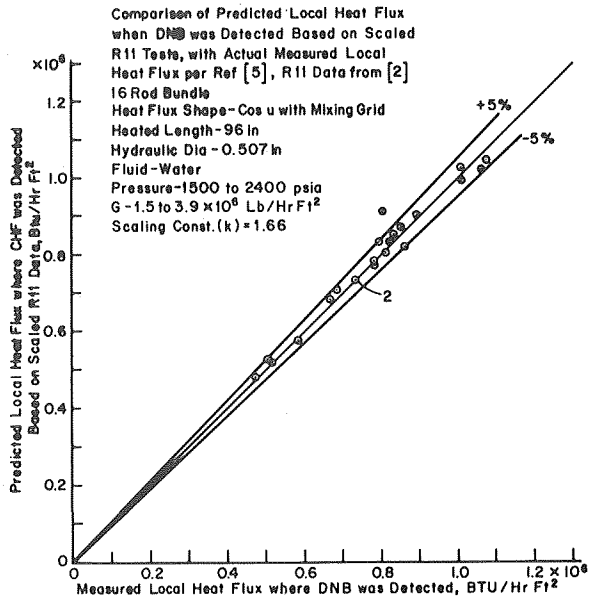

Fig. 2

Thermal Stresses in a Sphere Due to Local Heating Followed by Complete Cooling

T. S. Chen,[1] K. Thirumalai,[2] and J. B. Cheung[3]

Introduction

The present study was carried out to examine the response of rocks and related brittle solids to high energy surface heating fol-

[1] Department of Mechanical Engineering, University of Missouri-Rolla, Rolla, Mo. Mem. ASME

[2] Twin Cities Mining Research Center, U. S. Bureau of Mines, Twin Cities, Minn.

[3] Twin Cities Mining Research Center, U. S. Bureau of Mines, Twin Cities, Minn. Mem. ASME

Contributed by the Heat Transfer Division of The American Society of Mechanical Engineers. Manuscript received by the Heat Transfer Division November 28, 1973.

Downloaded from http://asmedigitalcollection.asme.org/heattransfer/article-pdf/97/1/145/5744399/145_1.pdf by Missouri University of Science & Technology user on 27 June 2023

 Copyright © 1975 by ASME

lowed by cooling and to evaluate the feasibility of its application to crushing hard rocks. This concept of weakening and breaking of rocks is known [1, 2],[4] but the supporting theoretical or experimental studies are not available in the literature.

Recent advances in high temperature technology provide high energy heaters such as the oxygen-fuel oil supersonic burners, high energy carbon arc and induction-type plasma heaters, lasers, and electron beam guns for industrial heating applications. These high energy heating tools are also suitable for localized rapid heating of rocks. Cooling can generally be achieved by quenching heated rocks.

The specific objectives of this brief are to extend the analysis of [3] to a cooling period that follows an initial heating period and to determine and interpret certain experimental results.

Analysis

Consider a homogeneous, isotropic, and elastic sphere of radius r_0, which is initially ($t \leq 0$) at zero reference temperature. During the time period $0 \leq t \leq t_H$, part of its spherical surface is subjected to axisymmetric heating with a prescribed surface heat flux $F(\theta)$, where the angle θ is measured from the axis of thermal symmetry. The unheated surface of the sphere is assumed to be insulated. For time $t \geq t_H$, the entire surface of the sphere is cooled in a fluid environment having heat transfer coefficient h and temperature T_∞. The temperature solution at time $t = t_H$ is derived in [3] and is denoted by $T(r, \mu, t_H)$, where $\mu = \cos\theta$ and r is the radial coordinate.

The temperature solution for the cooling period can be carried out in a manner similar to that for the heating period described in [3]. This gives

$$T(r, \mu, t^*) - T_\infty = \sum_{n=0}^{\infty}\sum_{m=1}^{\infty} \frac{(2n+1)\gamma_{nm}^2}{[\gamma_{nm}^2 - n(n+1) + B_i(B_i - 1)]J_{n+1/2}(\gamma_{nm})} \cdot \left\{\int_{-1}^{1}\int_{0}^{1} [T(r, \mu, t_H) - T_\infty] \frac{J_{n+1/2}\left(\frac{\gamma_{nm} r}{r_0}\right)}{r_0^2 r^{1/2}} P_n(\mu) r^2 dr d\mu\right\} \cdot \frac{J_{n+1/2}\left(\frac{\gamma_{nm} r}{r_0}\right)}{r^{1/2}} P_n(\mu) e^{-\kappa\gamma_{nm}^2 t^*/r_0^2} \quad (1)$$

where $t^* = t - t_H$, κ is thermal diffusivity, P_n is Legendre polynomial of degree n of the first kind, J_ν is Bessel function of the first kind of fractional order ν, γ_{nm} are the positive roots of

$$\gamma_{nm} J_{n-1/2}(\gamma_{nm}) = [(n+1) - B_i] J_{n+1/2}(\gamma_{nm}) \quad (2)$$

and

$$B_i = \frac{hr_0}{K} \quad (3)$$

is the Biot number.

The linear thermoelastic equilibrium equations and the stress displacement equations can be solved in conjunction with the traction-free condition $\sigma_{rr} = \sigma_{r\theta} = 0$ at $r = r_0$. The details of the solution method and the results for the case of heating are given in [3] and are, therefore, omitted here.

The expressions for the dimensionless radial stress $\tilde{\sigma}_{RR}$ and tangential stress $\tilde{\sigma}_{\theta\theta}$ during the subsequent cooling process are found to be

$$\tilde{\sigma}_{RR} = 2\sum_{n=0}^{\infty}\sum_{m=1}^{\infty} D_{nm}\left[\frac{2}{\gamma_{nm}R}\frac{J_{n-1/2}(\gamma_{nm}R)}{R^{1/2}} - \frac{(n+1)(n+2)}{\gamma_{nm}^2 R^2}\frac{J_{n+1/2}(\gamma_{nm}R)}{R^{1/2}}\right] P_n(\mu) e^{-\gamma_{nm}^2 \tau^*} + \sum_{n=2}^{\infty} n(n-1) a_n R^{n-2} P_n(\mu) + \sum_{n=1}^{\infty}(n+1)[(n+1)(n+2) - 2\nu] b_n R^n P_n(\mu) \quad (4)$$

$$\tilde{\sigma}_{\theta\theta} = -2\sum_{n=0}^{\infty}\sum_{m=1}^{\infty} D_{nm}\left\{\frac{J_{n-1/2}(\gamma_{nm}R)}{\gamma_{nm}R^{3/2}} P_n(\mu) + \left[\left(1 - \frac{n+1}{\gamma_{nm}^2 R^2}\right) P_n(\mu) - \frac{\mu}{\gamma_{nm}^2 R^2} P_n'(\mu) + \frac{1-\mu^2}{\gamma_{nm}^2 R^2} P_n''(\mu)\right] \times \frac{J_{n+1/2}(\gamma_{nm}R)}{R^{1/2}}\right\} e^{-\gamma_{nm}^2 \tau^*} + \sum_{n=2}^{\infty} a_n R^{n-2}[\mu P_n'(\mu) - n^2 P_n(\mu)] + \sum_{n=1}^{\infty} b_n R^n\{(n + 5 - 4\nu)\mu P_n'(\mu) - (n+1)[(n+1)^2 + 2(n+1) - 1 + 2\nu] P_n(\mu)\} \quad (5)$$

where $\tilde{\sigma}_{ij} = \sigma_{ij}/[G(1+\nu)q_0 r_0 \alpha/K(1-\nu)]$ with G, ν, α, *and* K denoting, respectively, shear modulus, Poisson's ratio, coefficient of thermal expansion, and thermal conductivity, $R = r/r_0$, $\tau^* = \kappa t^*/r_0^2$, $P_n' = dP_n/d\mu$, $P_n'' = d^2P_n/d\mu^2$,

$$D_{nm} = \frac{(2n+1)\gamma_{nm}^2}{[\gamma_{nm}^2 - n(n+1) + B_i(B_i - 1)]J_{n+1}^2{}_{/2}(\gamma_{nm})} \times \left[\int_{-1}^{1}\int_{0}^{1} \frac{T(r, \mu, t_H) - T_\infty}{q_0 r_0/K} \cdot \frac{J_{n+1/2}(\gamma_{nm}R)}{R^{1/2}} P_n(\mu) R^2 dR d\mu\right] \quad (6)$$

and

$$a_n = \frac{\eta_n[3n + 2 + 2\nu - n^3 + 2\nu n] + \xi_n[2 - (n+1)^2 - 2\nu]}{2(n-1)[n^2 + n + 1 + \nu(2n+1)]}, \quad n = 2, 3, \ldots \quad (7)$$

$$b_n = \frac{\xi_n + n\eta_n}{2[n^2 + n + 1 + \nu(2n+1)]}, \quad n = 0, 1, 2, \ldots \quad (8)$$

with

$$\xi_n(\tau^*) = -2\sum_{m=1}^{\infty} D_{nm}[n(n+1) + B_i]\frac{J_{n+1/2}(\gamma_{nm})}{\gamma_{nm}^2} e^{-\gamma_{nm}^2 \tau^*} \quad (9)$$

$$\eta_n(\tau^*) = -2\sum_{m=1}^{\infty} D_{nm}(1 + B_i)\frac{J_{n+1/2}(\gamma_{nm})}{\gamma_{nm}^2} e^{-\gamma_{nm}^2 \tau^*} \quad (10)$$

Results

To illustrate the results, Fig. 1 shows the computed tangential stress distributions $\sigma_{\theta\theta}$ for a 10 cm dia Sioux quartzite sphere heated under $q_0 = 0.95$ cal/cm^{2}s over its hemispherical surface ($\theta_0 = 90$ deg) for 30 s and then cooled over its entire surface for 30 s. The properties of the Sioux quartzite used in the calculations are $G = 8.79 \times 10^5$ N/cm^2, $K = 1.3 \times 10^{-2}$ cal/cm-s-°C, $\alpha = 1.25 \times 10^{-5}$ °C^{-1}, $\kappa = 2.5 \times 10^{-2}$ cm^2/s, and $\nu = 0.24$. An inspection of the figure reveals that tensile and compressive tangential stresses are induced, respectively, in the inner and outer region of the sphere during heating. The maximum tensile tangential stress is seen to have a magnitude of about 3000 N/cm^2 and to occur within about 2.7 cm from the spherical surface. The tensile strength of Sioux quartzite is about 2000 N/cm^2. The prescribed heating conditions will, therefore, provide the stress potential for fragmenting the rock specimen. In the subsequent cooling period, a stress reversal takes place in the outer layer of the sphere, giving tensile tangential stresses that are maximum at the surface and that progressively decrease in the interior of the sphere.

In the experiments, rock spheres of Sioux quartzite and Dresser basalt that are 10 cm in dia were insulated over the hemispherical surface and inserted in a radiative heat system controlled to transfer uniform heat flux into the spherical surface. The specimens

[4] Numbers in brackets designate References at end of paper.

Downloaded from http://asmedigitalcollection.asme.org/heattransfer/article-pdf/97/1/145/5744399/145_1.pdf by Missouri University of Science & Technology user on 27 June 2023

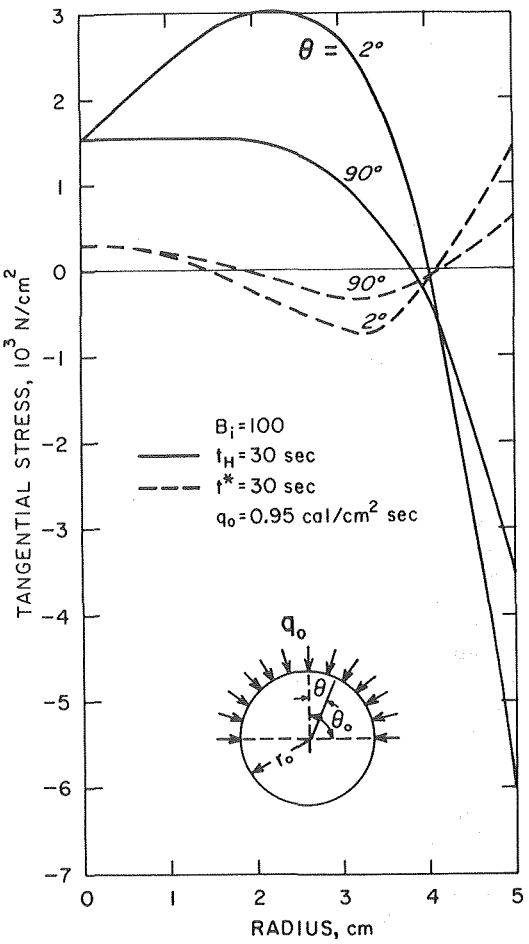

Fig. 1 Distribution of tangential stresses during partial heating and cooling of sioux quartzite

were heated over the exposed hemispherical surface at various constant fluxes until cracks were observed on the surfaces; the time periods for the crack occurrence were recorded. From these time periods, the corresponding maximum tensile tangential stresses were calculated. The results are presented in Fig. 2 with circles, and the analytically predicted maximum tensile tangential stresses versus time are illustrated with lines. It can be seen from the figure that the predicted tangential stresses in all cases exceed the tensile strength of the rock specimens and that the agreement between analysis and theory is very good. The locations of maximum tensile tangential stresses are the locations for crack initiation through the application of the tensile stress fracture criterion. The experimentally observed and analytically predicted locations of fracture initiation are shown in Fig. 3. The thickness of the broken pieces of rocks was found to be within 2–2.5 cm.

To examine the effect of cooling on fragmentation, spherical rock specimens that were insulated over the hemispherical surface were heated for short periods of time over the exposed surface such that complete fragmentation of the spheres did not take place during heating, and then were quenched with water. The results showed that cooling propagated fractures that were induced during heating in the interior of the sphere, but did not create new fractures at the specimen surface.

Concluding Remarks

The present analysis indicates that tensile stresses are induced in the interior of a sphere during heating and that subsequent cooling generates tensile tragential stresses at and close to the spherical surface. The internal tensile stress concentrations induced during heating create a potential for initiating fracture and fragmentation. From the experiments, it was found that fracture and fragmentation are confined to the surface area exposed to heating.

Rocks are weak in tension. Fragmentation of rocks by tensile stresses represents an efficient approach to breaking rocks. It is concluded from the present study that tensile stresses exceeding the strength of rocks can be induced in the interior of rocks by localized surface heating that produces fracture and fragmentation. Cooling of heated rocks augments fracture propagation and fragmentation but does not significantly vary the fragmentation characteristics induced by heating. The tensile stress concentrations in

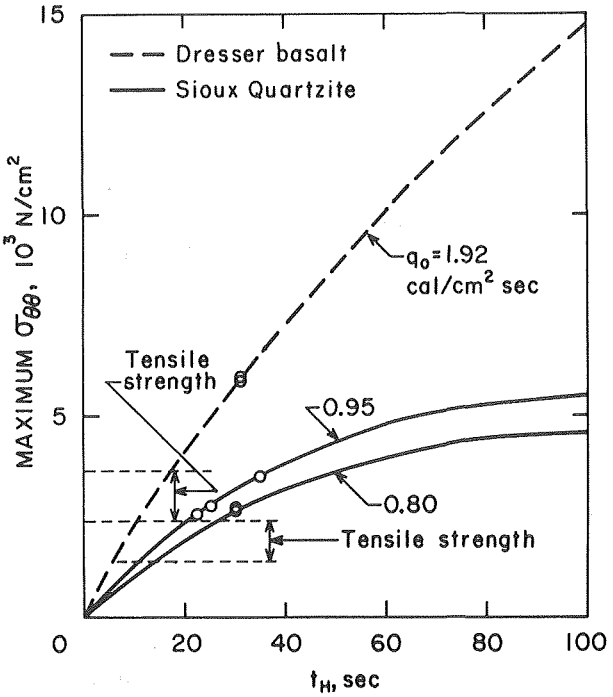

Fig. 2 Variation of maximum tensile tangential stress with heating time at $\theta = 2°$

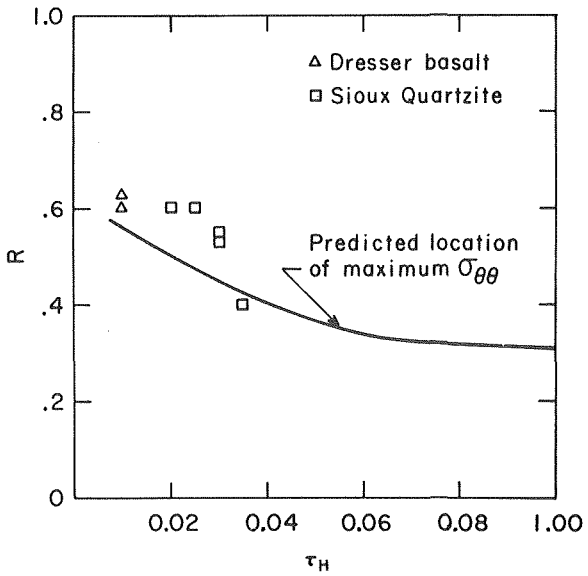

Fig. 3 Variation of location of maximum tensile tangential stress with heating time at $\theta = 2°$

Downloaded from http://asmedigitalcollection.asme.org/heattransfer/article-pdf/97/1/145/5744399/145_1.pdf by Missouri University of Science & Technology user on 27 June 2023

rock material flaws and microstructural cracks will play a dominant role in inducing fracture and fragmentation by heating and cooling.

Acknowledgments

This study was carried out by the Bureau of Mines in cooperation with the U. S. Army Mobility Equipment Research and Development Center (MERDC).

References

1 Thirumalai, K., "Potential of Internal Heating Method for Rock Fragmentation," *Proceedings of Twelfth Symposium on Rock Mechanics,* 1970, pp. 697–719.

2 Thirumalai, K., and Cheung, J. B., "A Study on a New Concept of Thermal Hard RocK Crushing," *Proceedings of Fourteenth Symposium on Rock Mechanics,* ASCE, 1972, pp. 527–554.

3 Cheung, J. B., Chen, T. S., and Thirumalai, K., "Transient Thermal Stresses in a Sphere by Local Heating," *Journal of Applied Mechanics,* TRANS. ASME (in press); see also ASME Paper No. 74-WA/APM-9.

Heating Time and Heating Temperature Dependence of Thermal Conductivity of As-Received Aluminum Alloy 2024-T351

S. Al-Araji[1] and J. V. Beck[2]

1 Introduction

When as-received aluminum alloy 2024-T351 is heated to 350°F (450°K), changes in the microstructure take place. These changes are further enhanced by heating to higher temperatures and/or for longer times. This heating results in increases in the room-temperature values of the thermal conductivity *(k)* of the alloy. These changes are functions of the heating temperature and also of the heating time because the microstructure changes with time. No data are known to be extant showing heating time as well as heating temperature variations of k for aluminum alloy 2024-T351. However, there are data in the literature concerning time at temperature effects on the properties of some materials [1, 2].[3]

This work is important for several reasons. First, the data for this particular alloy are needed for such applications as nuclear reactors, where this material, if used, might be exposed to a sudden heating condition. Next, the experimental procedure and the demonstration of a successful application of it is significant. Finally, there are many other materials which change during heating. These include biological products which dry and otherwise change during slow heating. The techniques mentioned in this study might also be applicable to such cases.

A simplified method proposed by Beck and Al-Araji [3] was used to determine the transient values of k.

2 Experiment

The specimen is made of aluminum alloy 2024-T351, which is composed of aluminum, 3.8–4.9 percent copper, 0.50 percent silicon, 0.50 percent iron, 0.3–0.9 percent manganese, 1.2–1.8 percent magnesium, 0.10 percent chromium, 0.25 percent zinc, and 0.15 percent others. It is solution heat-treated and stress-relieved.

Because of the particular structure of the alloy, the experimental strategy was developed [4] to be as follows: (1) testing the specimen at room temperature, (2) heating the specimen to and holding it at the desired temperature, then performing the tests, and (3) cooling the specimen down to room temperature and testing it at that temperature. That is, the specimen is tested first at room temperature conditions to determine its thermal conductivity in the as-received state, then heated to the desired temperature and held at that temperature until it is over-aged. During this period the thermal conductivity of the specimen is determined at different intervals of time. The time intervals between tests are determined by the temperature level at which the specimen is held. The higher the temperature at which the specimen is maintained, the more rapidly the specimen reaches its over-aged condition.

3 Experimental Results

Twelve specimens were tested in the temperature range 375–425°F (464–491°K) to find the k values in that temperature range.

The thermal conductivity values obtained using this method of testing are compared with those compiled by the Thermophysical Properties Research Center (TPRC) [5] in Fig. 1.

It should be noted that the values given by TPRC are for aluminum alloy 2024-T4, the same alloy but with a different initial heat treatment designated by "T4," which indicates that the alloy had been solution heat-treated and naturally aged to a substantially stable condition. This difference in initial heat treatments might account for the difference between the TPRC values and the present results.

The lower dashed line in Fig. 1 depicts the initial values (zero-time) of k in the present study; zero-time values are given from room temperature (about 540°R or 300°K) to about 885°R or 491°K. The final values of k (over-aged values) found in the present study are depicted by the upper dashed line for the same temperature range. Note that Fig. 1 shows that the k value at room temperature for the over-aged condition is much higher than that in the as-received condition, while that for the temperature at 491°K is not.

Details of the time variation of the thermal conductivity k suggested by Fig. 1 are interesting. Just below 350°F (450°K) it takes several days for changes in the properties to occur. Below 300°F (422°K) it may take weeks or months; we did not investigate this range. The average k values for all specimens tested in the temperature range 375–425°F (464–491°K) are shown in Fig. 2. These values seem to exhibit a certain pattern. This pattern begins with the k value of the specimen when it is first brought to its nominal temperature; then k increases to some maximum value while the specimen is maintained at the nominal temperature. The rate of increase of the thermal conductivity depends on the temperature level, with the higher temperatures causing more rapid changes in

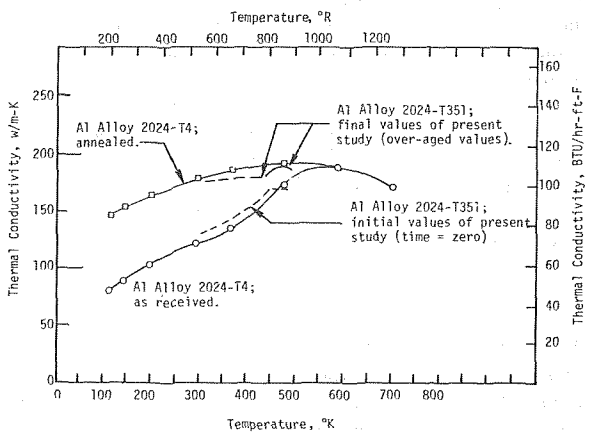

Fig. 1 Thermal conductivity of aluminum alloy 2024-T4 given by TPRC [5] and of aluminum alloy 2024-T351 of present study

[1] Instructor (now with the Consumers Power Co.; Jackson, Mich.) Department of Mechanical Engineering, Michigan State University, E. Lansing, Mich.

[2] Professor, Department of Mechanical Engineering and Division of Engineering Research, Michigan State University, E. Lansing, Mich.

[3] Numbers in brackets designate References at end of technical brief.

Contributed by the Heat Transfer Division of THE AMERICAN SOCIETY OF MECHANICAL ENGINEERS. Manuscript received by the Heat Transfer Division June 28, 1974.

Downloaded from http://asmedigitalcollection.asme.org/heattransfer/article-pdf/97/1/145/5744399/145_1.pdf by Missouri University of Science & Technology user on 27 June 2023